White Rose Research Online

eprints@whiterose.ac.uk
https://eprints.whiterose.ac.uk
Universities of Leeds, Sheffield and York

Deposited via The University of Leeds.

White Rose Research Online URL for this paper:
https://eprints.whiterose.ac.uk/id/eprint/245820/

Version: Accepted Version

Article:
Wu, W., Chen, Y.-T. and Wanatowski, D. (2026) Long-term deformation mechanisms of double-track heavy-haul railway embankment under bidirectional shear loadings. Acta Geotechnica. ISSN: 1861-1125

https://doi.org/10.1007/s11440-026-03064-9

This is an author produced version of an article published in Acta Geotechnica, made available via the University of Leeds Research Outputs Policy under the terms of the Creative Commons Attribution License (CC-BY), which permits unrestricted use, distribution and reproduction in any medium, provided the original work is properly cited.

Reuse
This article is distributed under the terms of the Creative Commons Attribution (CC BY) licence. This licence allows you to distribute, remix, tweak, and build upon the work, even commercially, as long as you credit the authors for the original work. More information and the full terms of the licence here:
https://creativecommons.org/licenses/

Takedown
If you consider content in White Rose Research Online to be in breach of UK law, please notify us by emailing eprints@whiterose.ac.uk including the URL of the record and the reason for the withdrawal request.

UNIVERSITY OF LEEDS
University of Sheffield
UNIVERSITY of York

Long-term deformation mechanisms of double-track heavy haul railway embankment under bi-directional shear loadings

Weipin Wu[1], Yung-Tsang Chen[1*], Dariusz Wanatowski[2]

[1]Department of Civil Engineering, University of Nottingham, 199 Taikang East Road, Ningbo, 315100, China.
[2]Faculty of Engineering and Physical Sciences, University of Leeds, Woodhouse Lane, Leeds, LS2 9JT, United Kingdom.

*Corresponding author(s). E-mail(s): Yung-Tsang.Chen@nottingham.edu.cn;

Abstract

During heavy-haul train crossings, embankments develop complex stress paths characterized by bi-directional principal stress rotation (PSR) spanning centerline, unloaded-track, and loaded-track zones. Assessing the long-term embankment deformation under cyclic traffic loading without considering the bi-direction PSR effect may result in under-estimation of the soil deformation. This study investigates the deformation mechanisms of double-track heavy haul railway embankments subjected to cyclic traffic loading. Utilizing finite element simulated critical stress paths extracted from embankment cross-sections, the uni- and bi-directional PSR scenarios are compared explicitly using variable-direction dynamic cyclic simple shear (VDDCSS) experiments. Results indicate that bi-directional PSR generate stress path across 3D space, contrasting with the single-plane confinement of uni-directional PSR. For equivalent depths underneath the tracks, vertical displacements under bi-directional PSR surpass uni-directional PSR values at both the embankment center and loaded line areas. Findings from this study demonstrate that bi-directional PSR modeling is crucial for accurately predicting the long-term settlement of heavy-haul railway embankments under cyclic traffic loads.

Keywords: Bi-directional shear loading; double-track rail embankment; heavy haul railway; long-term deformation

1 Introduction

Originating in the United States during the 1920s, heavy-haul rail transport has a development history of more than a century; heavy-haul rail systems have become essential for long-distance transportation of bulk commodities such as mineral resources and energy materials [1–4]. However, the amplitude and duration of train dynamic loads on heavy-duty railway foundations significantly increase with the increase of axle load, total weight, traffic density, and traffic volume [5], which has been recognized as a primary driver of sustained post-construction deformation in railway substructures. This results in life-cycle operational expenditures consistently surpassing initial infrastructure investments in heavy haul corridor economic evaluations, particularly regarding track system durability [6, 7]. Empirical data analysis reveals that trackbed rehabilitation constitutes over 60% of long-term maintenance budgets, as documented in permanent way deterioration studies [8]. Operational loading frequency emerges as a critical design parameter for substructure engineering, given that cyclic stress applications from high-mass rolling stock accelerate component fatigue and induce cumulative deformation mechanisms in both superstructure elements and subgrade materials [9]. This operational reality underscores the necessity for comprehensive foundation analysis methodologies that concurrently evaluate axle load magnitude and traffic frequency parameters, enabling optimized geotechnical designs that mitigate degradation rates while controlling preservation costs across the infrastructure life-cycle.

Track foundation maintenance decisions fundamentally rely on accurate assessment of settlement magnitudes, where conventional evaluation methods have employed cyclic load count as the primary predictor of vertical strain development. Traditional assessment techniques derived from empirical correlations in cyclic triaxial testing [10–14] typically model vertical deformation through simplified axial stress approximations across foundation layers. These approaches exhibit inherent limitations due to their oversimplified stress representation, failing to capture the complex multiaxial stress conditions generated by moving train loads, particularly the persistent principal stress axis rotation (PSR) phenomenon. Research demonstrates that neglecting three-dimensional stress evolution, especially PSR effects, leads to systematic underestimation of long-term settlement in transportation infrastructure foundations [15–17].

Emerging research in transportation geotechnics underscores the necessity of accounting for PSR in foundation analysis under complex loading conditions [16–19]. Current experimental methodologies for evaluating track foundation deformation employ hollow cylindrical apparatus (HCA) systems that simulate uni-directional PSR, offering improved simulation fidelity over conventional triaxial setups by better replicating in-situ stress paths under cyclic loading [20–25]. However, soil experiences simultaneous stress axis rotations along both the train movement direction and its orthogonal plane during actual operations, generating a “bi-directional PSR” mechanism. Conventional HCA configurations cannot replicate this coupled rotational behavior due to inherent limitations in their stress application mechanisms [10]. To address this, the variable-direction dynamic cyclic simple shear (VDDCSS) system was developed, enabling independent control of dynamic normal stress and bi-directional

shear stresses [26]. This innovation permits full simulation of traffic-induced bi-axial stress rotations, providing enhanced capability to quantify permanent deformation mechanisms in foundation soils under realistic loading patterns.

Heavy-haul railway embankments typically require longer slopes compared to conventional railways especially for double track heavy haul railway, causing larger thickness of each embankment layers, generating significant initial static shear stresses in the horizontal plane perpendicular to traffic direction due to their substantial self-weight. These initial static shear stresses become further intensified under the high axle loads characteristic of heavy-haul operations. Recent VDDCSS experimental studies [27–31] have demonstrated that such pre-existing initial static shear stresses critically influence soil strain development patterns. However, the specific effects of these initial static shear stresses on deformation behavior in heavy-haul railway embankments under actual train loading conditions remain unexplored, particularly regarding the interaction between inherent embankment gravity induced shear stresses and dynamic wheel-rail forces induced bi-directional PSR.

Research on soil deformation mechanisms in heavy-haul railway subgrades has advanced through improved experimental methods. Gräbe et al. [32] compared triaxial and HCA tests, revealing that triaxial tests underestimate permanent strain development compared to field data, whereas HCA tests incorporating PSR better simulate permanent strain accumulation. Their findings highlight PSR's critical role in subgrade deformation under cyclic loading. Leng et al. [33] performed triaxial tests on over 30 types of embankment materials, analyzing cumulative permanent strain while considering moisture content and confining pressure. They derived empirical formulas for resilient modulus and permanent axial strain to aid in embankment design. Zhao et al. [34] conducted dynamic triaxial tests on fiber-reinforced soil, demonstrating that confining pressure and fiber content significantly improve its dynamic properties, offering enhanced durability under heavy traffic loads. Despite these advances, existing studies have not accounted for bi-directional PSR due to equipment limitations. Neglecting this effect may lead to underestimating vertical embankment deformation, which warrants further investigation.

This study investigates soil deformation in railway embankments under heavy-haul traffic loads, incorporating the effects of initial static shear stress and bi-directional PSR. To accurately capture the stress path induced by train movement, a finite element model (FEM) simulates the complete passage of heavy-haul trains on a double-track line. The derived stress paths representing normal and shear stress amplitudes and waveforms at various subgrade locations are then replicated in a VDDCSS tester to assess deformation characteristics, resilient modulus evolution, and shear stress distribution. Comparative analysis reveals that bi-directional PSR induces greater soil deformation than uni-directional PSR, highlighting its critical role in long-term embankment behavior. These results enhance the understanding of cyclic traffic load effects on subgrade stability, offering valuable insights for the design and maintenance of heavy-haul railway infrastructure.

2 Stress path analysis through numerical simulation

2.1 Finite element model specifications

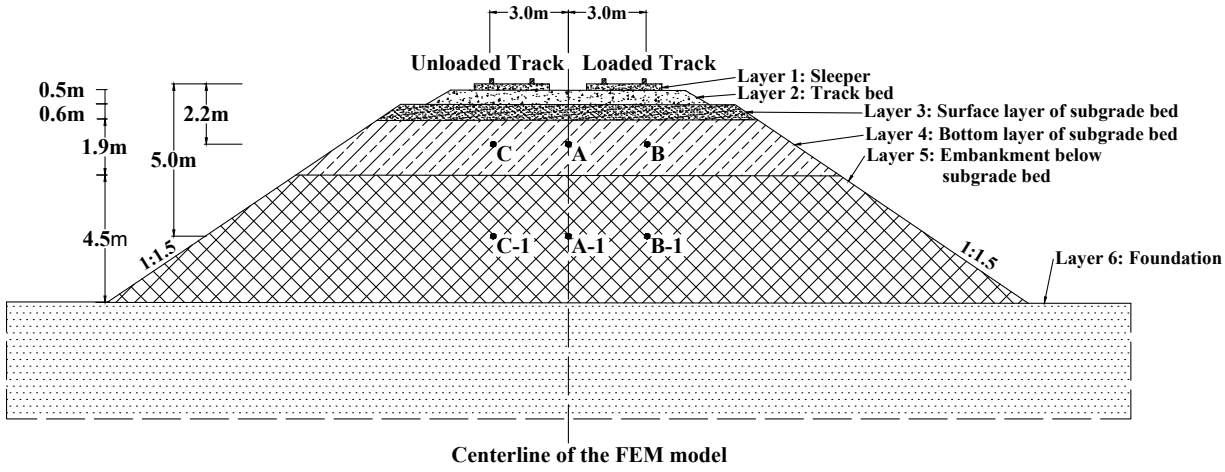


Fig. 1 Cross-section of a typical dual-track heavy-haul railway embankment.

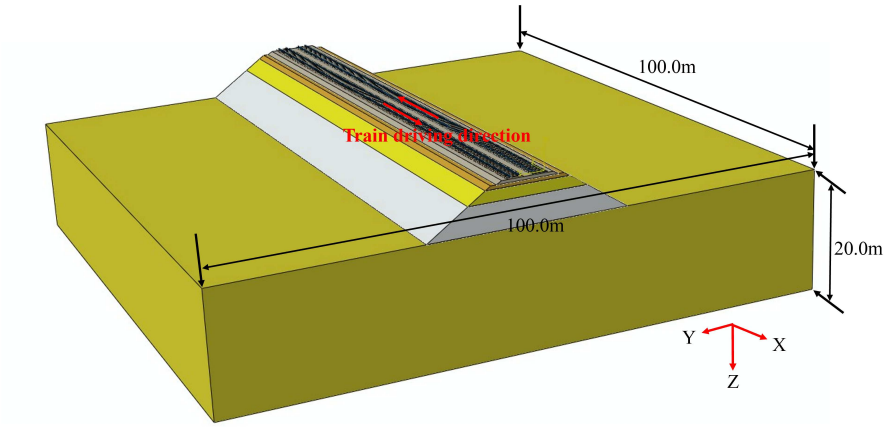


Fig. 2 FEM model of the double track railway embankment and foundation.

To investigate the stress paths due to complex railway traffic loads, a typical railway embankment taken from the Shuo Huang heavy-haul railway in China, as shown in Fig. 1, was selected. Deformations of the dual-track railway embankment in dynamic conditions (moving trains) were first studied in 3D formulation using ABAQUS [35],

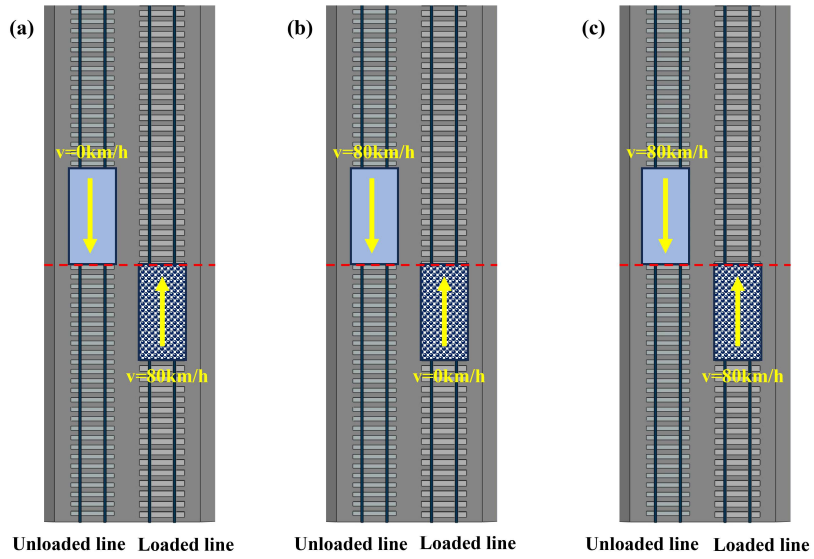


Fig. 3 Top view of the simulated train loads in the FEM model.

Table 1 Material properties of the railway embankment used in the FEM model.

Layer No.	Layer Name	Density (kg/m^3)	Elastic Modulus (MPa)	Poisson's Ratio	Friction Angle (°)	Cohesion (kPa)
	Rail	7850	200000	0.30	-	-
1	Sleeper	2500	32500	0.18	-	-
2	Track bed	2200	250	0.25	-	-
3	Surface layer	2000	180	0.33	30	80
4	Bottom layer	2000	120	0.33	28	72
5	Embankment	1850	100	0.35	25	60
6	Foundation	1800	80	0.35	20	54

as illustrated in Fig. 2. In the simulated double track heavy-haul railway embankment, one track is assumed as full-loaded from the outward train with goods, while the other track is assumed empty-loaded from the return train. In order to simulate more realistically the operating conditions, three scenarios were chosen, as shown in the Fig. 3, and it was assumed in these scenarios that the outward and return trains met at the midpoint of the model. More specifically, the first scenario simulates the loaded (outward) train is running at a specified speed, while the unloaded (return) train is stationary. The second scenario assumes the unloaded train is running while the loaded train has stopped. The third scenario is set for both trains running at a constant speed simultaneously.

Given that the analysis targets the stress state induced by a single train passage, where the soil response is predominantly elastic, the extracted PSR geometry is not sensitive to the specific constitutive model for this first-cycle simulation ([36, 37]).

In accordance with the actual mechanical performance of track structures, the sleepers and track beds were represented by a linear elastic constitutive model. For the underlying subgrade soils, whose response involves both recoverable and permanent deformations, the Mohr-Coulomb elastoplastic model was employed. The material parameters for each embankment layer, summarized in Table 1, were determined based on the design specifications for railway earth structures outlined in the Chinese code TB 10625-2017 [40], and were further validated against established findings in the literature [41–43]. The embankment model with its soil layers and dimensions is shown in Fig. 1, while the material properties of each layer are summarized in Table 1.

This study mainly observes the mechanical behavior of embankments; therefore, in order to balance simulation accuracy and computational efficiency, a dense grid was divided in the embankment section (core mesh area), and the grid density gradually decreased in the foundation section far away from the embankment. The model included 66,625 C3D8R elements, and the two observed soil filling embankment layers (i.e. Layers 4 and 5 in Fig. 1) were all in the core mesh area for simulation accuracy.

The Chinese C96 heavy-haul trains were applied as traffic loads on the track, with wheel load dimensions illustrated in Fig. 4. The C96 load model consists of quadruple 300 kN axle groups (equivalent to 30-tonne axle loads) for fully loaded trains and a corresponding unloaded configuration with 60 kN axle loads (6 tonnes/axle). The front and rear axle sets are longitudinally spaced at 11.66 m under identical geometric configurations. Quasi-static loads dominate the foundation response in heavy-haul operations, as wheel-impact vibrations attenuate rapidly with depth, which is consistent with the findings of Tang et al. [44].

The moving train load was simulated using a D-load subroutine in ABAQUS. A Fortran-coded subroutine controlled eight concentrated wheel loads moving at 80 km/h. Each wheel load was applied as a uniform pressure over a circular area (diameter equal to sleeper width) on the ballast surface. To minimize boundary reflections, the model domain was made substantially large (28 m deep, 60 m wide), ensuring boundaries were distant enough not to influence stresses in the observation zones during the short loading event.

The stress paths were evaluated at specific locations in the embankment soil layers as illustrated in Fig. 1. The embankment was modeled as a symmetrical structure, with analysis conducted on the right half. Six monitoring points (A, B, C and their corresponding -1 counterparts) were strategically placed in the cross-section at two distinct depths: 2.2 m (points A-C) and 5.0 m (points A-1 to C-1). points A and A-1 were positioned directly beneath the embankment centerline. points B and B-1 were placed 3.0 m laterally from the centerline, aligned vertically with the outer rail of the loaded track. Similarly, points C and C-1 were located 3.0 m from the centerline but beneath the outer rail of the unloaded track. This arrangement enabled comparative analysis of stress distributions under different loading conditions while maintaining consistent geometric relationships between measurement locations.

2.2 Analysis of numerical simulation results

This section presents the results of FEM simulations, with a particular focus on the stress path waveforms induced by the passage of a heavy haul train on a double-track

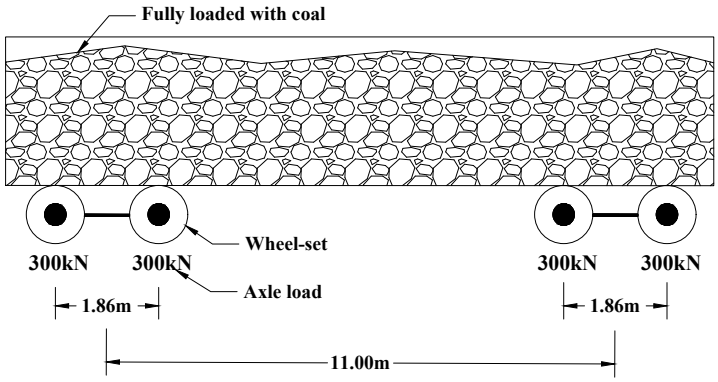


Fig. 4 Spatial distribution of wheel axles for a heavy-haul train (Type C96).

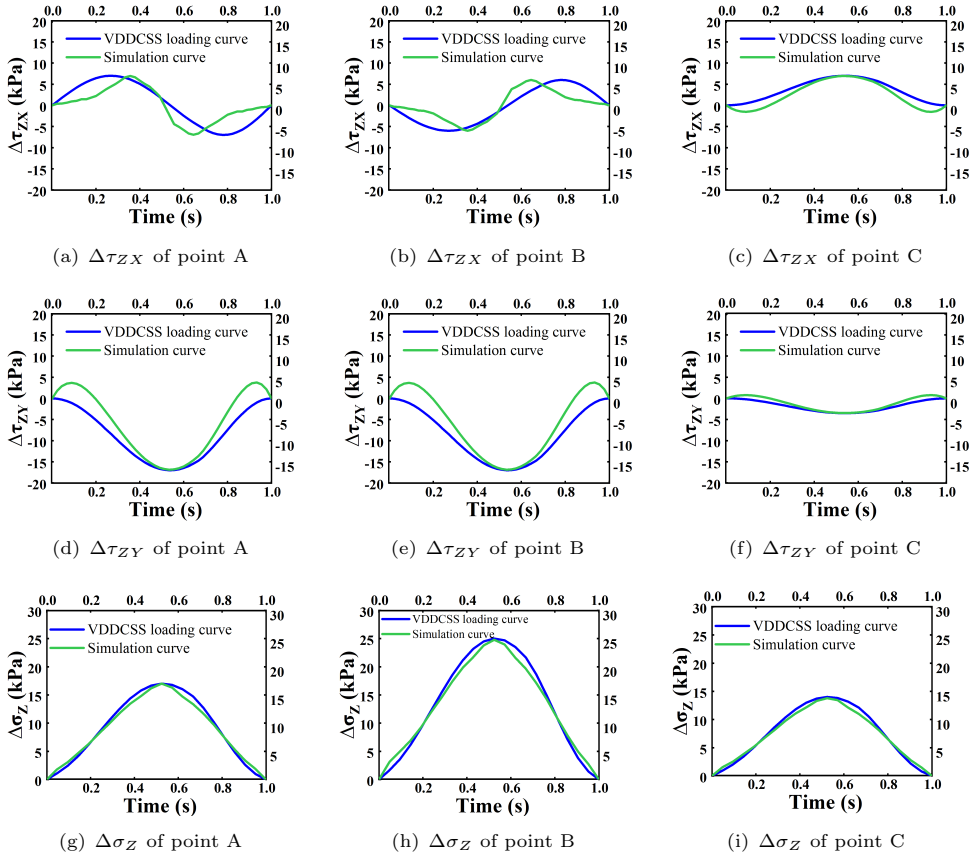
Table 2 Results of the stress paths from the FEM simulation.

point No.	σ_Z (kPa)	Initial τ_{ZY} (kPa)	$\Delta\sigma_Z$ (kPa)	$\Delta\tau_{ZX}$ (kPa)	$\Delta\tau_{ZY}$ (kPa)
A	100	0	17	7	-17
A0	100	0	17	7	0
B	100	-30	25	8	-17
B0	100	-30	25	8	0
C	100	-30	14	6	-3.5
C0	100	-30	14	6	0
A-1	200	0	13	5	-7
A0-1	200	0	13	5	0
B-1	200	-10	20	5	-6
B0-1	200	-10	20	5	0
C-1	200	-10	5	1.5	-2.5
C0-1	200	-10	5	1.5	0

heavy haul railway. The most unfavorable simulation results (Scenario 3 in Fig. 3) of the embankment induced by cyclic traffic loading were presented. Table 2 shows the results of the stress paths from the FEM simulation. It is important to note that, to investigate the bi-directional versus uni-directional PSR effects, paired comparative cases were established such that each bi-directional PSR case (A, B, C, A-1, B-1, C-1 with considering Y-direction shear stress (τ_{ZY})) was assigned a corresponding uni-directional counterpart (A0 for A, B0 for B, C0 for C, A0-1 for A-1, B0-1 for B-1, and C0-1 for C-1) where the counterparts preserved identical stress amplitudes but eliminated Y-direction shear stress ($\tau_{ZY} = 0$), thereby serving as reference baselines. Since the stress path waveforms at deeper points (A-1, B-1, C-1) are identical to their shallow counterparts (A, B, C), the analysis below focuses on the points of 2.2 m depth.

2.2.1 Analysis of stress wave propagation

Fig. 5(a)-5(f) presents the shear stress waveforms and corresponding amplitudes at observation points A, B, and C, extracted along both X- and Y-directions on the horizontal plane. The dynamic shear stress waveforms from the FEM analysis (green traces, simulation curve) exhibited distinct directional characteristics: in the X-direction, observation points A and B (as shown in Figs. 5(a) and 5(b), respectively) demonstrated quasi-sinusoidal periodic variations on $\Delta\tau_{ZX}$, whereas point C (Fig. 5(c)) displayed a different waveform pattern. Conversely, in the Y-direction, all three observation points (A, B, and C) manifested similar shear stress waveforms on $\Delta\tau_{ZY}$, as shown in Figs. 5(d)-5(f), differing primarily in magnitude of their amplitude oscillations. These results show spatial dependence of shear stress evolution relative to track embankment geometry.



(a) $\Delta\tau_{ZX}$ of point A (b) $\Delta\tau_{ZX}$ of point B (c) $\Delta\tau_{ZX}$ of point C

(d) $\Delta\tau_{ZY}$ of point A (e) $\Delta\tau_{ZY}$ of point B (f) $\Delta\tau_{ZY}$ of point C

(g) $\Delta\sigma_Z$ of point A (h) $\Delta\sigma_Z$ of point B (i) $\Delta\sigma_Z$ of point C

Fig. 5 Shear and normal stress waveforms per loading cycle for different observation points.

Normal and shear stresses share similar waveforms. Fig. 5(g) illustrates normal stress waveforms at point A, with Fig. 5(h) and 5(i) presenting analogous measurements for points B and C, respectively. Collectively, these diagrams confirm the waveform reproduction reliability of the VDDCSS. As evidenced in Fig. 5, experimentally recorded profiles (blue traces, VDDCSS loading curve) derived from enhanced harmonic fitting methodologies exhibit good correspondence with FEM modeling outputs.

2.2.2 Analysis of principal stress rotation

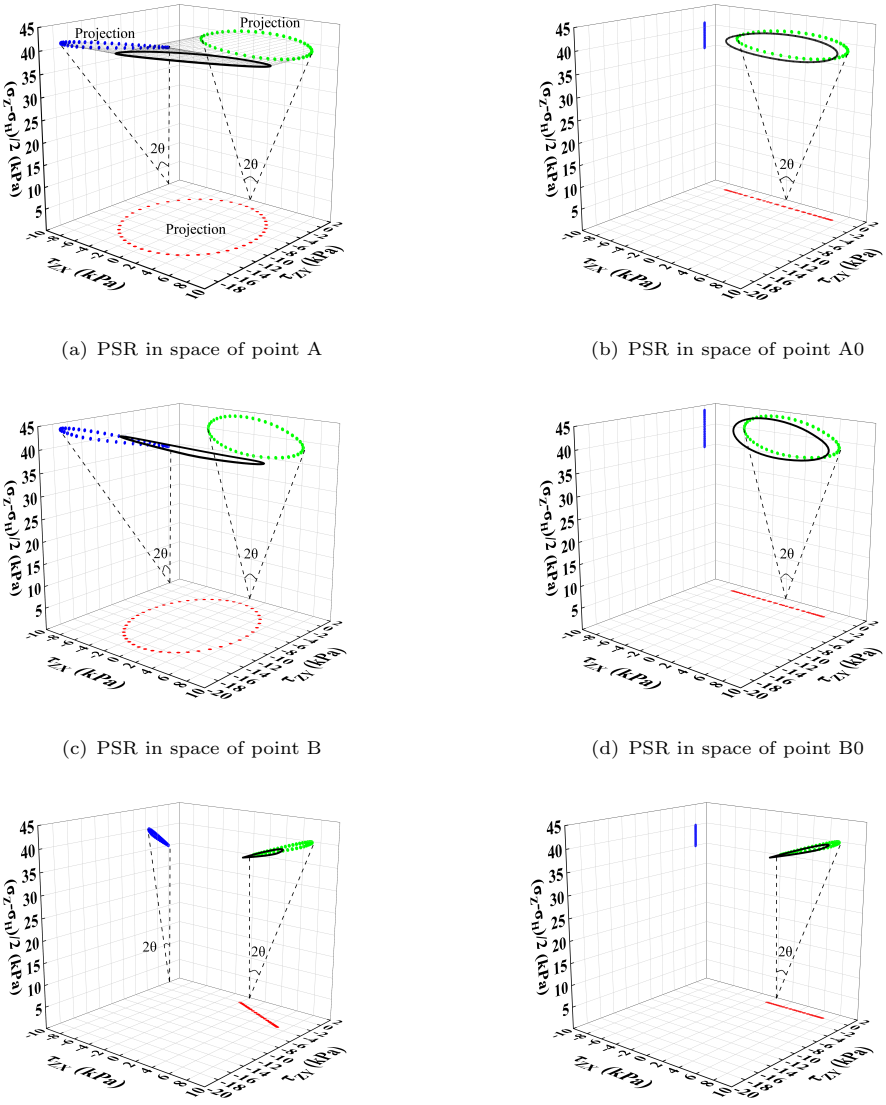
The FEM analysis identifies both uni- and bi- directional principal stress rotations. Fig. 6 shows the deviated stress paths and VDDCSS loading paths within the $\tau_{ZX} - \tau_{ZY} - (\sigma_Z - \sigma_X)/2$ stress space. It can be seen from the figure that monitoring points A, B and C (Figs. 6(a), 6(c) and6(e)) consistently exhibit bi-directional PSRs, as evidenced by rotational patterns in both X-Z (green traces) and Y-Z (blue traces) plane projections of their spatial stress paths, while both projections show oval shape. On the contrary, counterpart points A0, B0 and C0 (Figs. 6(b), 6(d) and 6(f)) demonstrate uni-directional PSR with rotations confined exclusively to the X-Z plane, clearly observable through the absence of rotational signatures in their Y-Z projections. And in the X-Z plane, the projection of uni-directional PSR condition display a vertical line. Both bi- and uni-directional PSRs in space project the shear stress path in the X-Y plane as shown in the red trace. Similar to the projection in the Y-Z plane, the shape of the projection in the X-Y plane displays two distinct types: elliptical or flattened approaching linear, since stresses exist in both X and Y directions. These fundamentally distinct PSR behaviors are further revealed through comparative analysis of deviatoric stress paths.

It is pivotal to note that the effects of soil's self-weight should be taken into account in these paths, with Shuo Huang Railway simulations establishing vertical normal stresses of 100 kPa at points A to C and A0 to C0, versus 200 kPa at their deeper equivalents (A-1 to C-1 and A0-1 to C0-1). The consolidation stress σ_Z for VDDCSS path derivation is derived from these normal stress values, while σ_X calculation methodology is comprehensively developed in the subsequent section.

3 Experimental program

3.1 Test setup and sample preparation

Experimental evaluation of PSR effects was performed using the VDDCSS apparatus, the first commercial solution for multi-directional shear testing, enabling controlled studies of both uni- and bi-directional principle stress rotation, as shown in Fig. 7. The VDDCSS represents an evolutionary advancement of the NGI-type simple shear apparatus originally developed by GDS Instruments (UK). This next-generation system replaces conventional hydraulic actuation with three independent electromechanical actuators, enabling precise simulation of complex multi-directional loading conditions. The system employs orthogonal X/Y electromechanical actuators that allow fully decoupled shear stress control, automated through GDALAB software.



(a) PSR in space of point A

(b) PSR in space of point A0

(c) PSR in space of point B

(d) PSR in space of point B0

(e) PSR in space of point C

(f) PSR in space of point C0

Fig. 6 PSR in space of different observation points.

This investigation examined the dynamic response of Leighton Buzzard sand under complex stress paths using multi-parameter cyclic testing. Specimens were prepared using Leighton Buzzard Sand (Fraction E) with void ratios $e_{\max} = 1.014$, $e_{\min} = 0.613$ [45]. Cylindrical specimens (70 mm in diameter and 17 mm in height) were employed to minimize stress/strain non-uniformity, adhering to established experimental design protocols by Boulanger and Seed [46] and Kim [47]. The VDDCSS replicated target

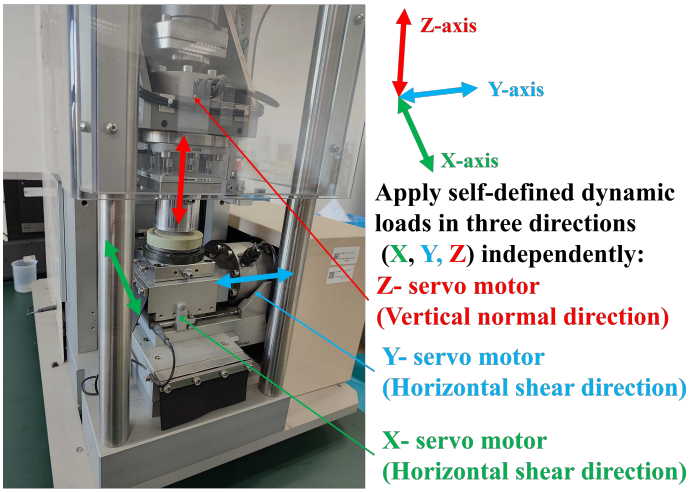


Fig. 7 Dynamic loading diagram of VDDCSS.

normal and shear stress waveforms, with numerical validation presented in Section 2.2.1. Soil specimens from various locations were initially consolidated under specified conditions. Subsequently, traffic-load induced stress paths (represented by blue lines in Figs. 5) were applied. Numerical simulations indicated distinct vertical stress conditions: 100 kPa at surface measurement points (A-C, A0-C0), doubling to 200 kPa at their matching -1 locations.

3.2 Normal stress in lateral direction

Since the VDDCSS apparatus cannot directly regulate lateral normal stress, Wood et al. [48] proposed an alternative experimental approach using a Cambridge-type simple shear device. Their methodology involved testing Leighton Buzzard sand under dynamic loading conditions to establish a direct correlation between vertical and lateral stresses; the correlation is given below:

$$\sigma_H = \frac{\tau^2}{(1 - K_0)\sigma_Z} + K_0\sigma_Z \tag{1}$$

where:
σ_H = lateral normal stress (kPa), σ_Z = vertical normal stress (kPa), τ = total shear stress, K_0 = static earth pressure coefficient.

The coefficient K_0 depends on the soil's friction angle φ [49, 50]:

$$K_0 = 1 - \sin\varphi \tag{2}$$

For Leighton Buzzard sand fraction E, $\varphi = 39.4°$ [51].

The lateral normal stress in this study is calculated using Eqs. (1) and (2).

3.3 Testing plan

To investigate soil deformation under heavy-haul railway loading conditions, cyclic tests incorporating both uni- and bi-directional PSR were performed. The experimental program, detailed in Table 2, examined three critical bi-directional PSR stress paths (points A, B, C) along with their uni-directional PSR counterparts (points A0, B0, C0), all derived from finite element modeling results. To ensure reliability, parallel paths (points A-1, B-1, C-1) and corresponding uni-directional cases (points A0-1, B0-1, C0-1) were included for comparative analysis. This systematic approach enabled comprehensive evaluation of soil mechanical behavior under complex, realistic loading conditions representative of long-term traffic effects.

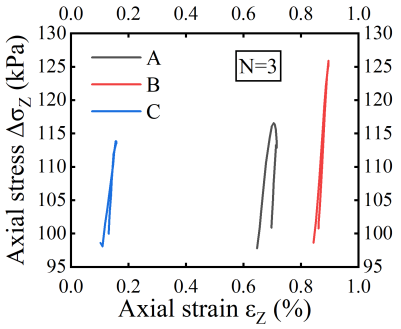
The primary cyclic tests employed a loading frequency of 1 Hz. This frequency was chosen as it lies within the expected range for traffic loading (0.5-5 Hz) and matches the frequency used in relevant studies [36, 52–55]. To investigate the influence of loading frequency, an additional test was conducted on the stress path of point A at 0.8 Hz (corresponding to a train speed of 64 km/h). Implementation of the specific cyclic stress functions defined for each stress path, guided by the waveforms in Figs. 5, was achieved within the device by controlling the stress components according to the values specified in Table 2.

4 Results and analysis

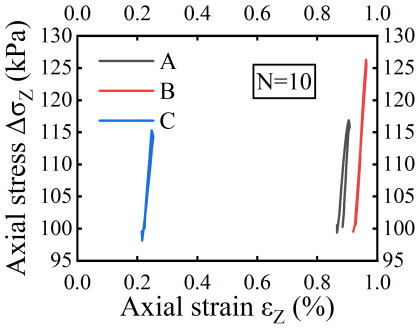
4.1 Bi-directional PSR effects on stress-strain behavior

The axial stress-strain responses under bi-directional (paths A, B, C) and uni-directional PSR (paths A0, B0, C0) conditions are compared in Fig. 8. A distinct difference in hysteresis evolution is observed: the hysteresis loops under bi-directional PSR narrow progressively with cycling, indicating rapid initial fabric stabilization and strain accumulation. In contrast, loops under uni-directional PSR remain consistently wider, accompanied by a slower strain development rate. For instance, at point B (Fig. 8(a), 8(d)), the axial strain under bi-directional PSR reaches 0.86% by the 3rd cycle and stabilizes at 2.39% after 5000 cycles. Under uni-directional PSR (point B0, Fig. 8(e), 8(h)), the corresponding values are only 0.18% and 1.48%, respectively. This demonstrates that bi-directional PSR accelerates particle rearrangement and densification.

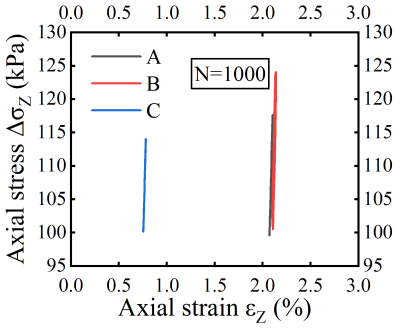
Fig. 9 shows the shear stress-strain development of points A, B and C. It can be seen from the figure that, in the Y-Z plane shear strain evolution (Figs. 9(e)-9(h)), the strain increases with increasing loading cycles. In contrast, the shear stress-strain relationship in the X-Z plane for points A and B (Figs. 9(a)-9(d)) displays almost no unidirectional strain accumulation, for the reason that the soil was subjected to periodic shear stress τ_{ZX}. However, the shear strain in the X-Z plane for point C shows slight strain accumulation particularly from N=10 to N=1000, as shown in the Figs. 9(b)-9(c); this is due to different stress path with points A and B as shown in Figs. 5 (a)-(c).



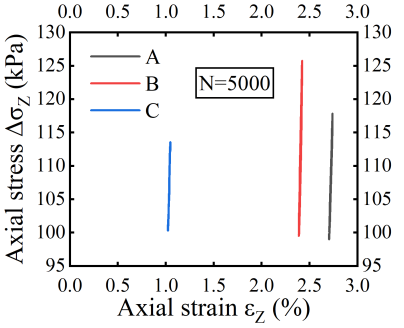
(a) Bi-directional PSR for typical cycle (N=3).



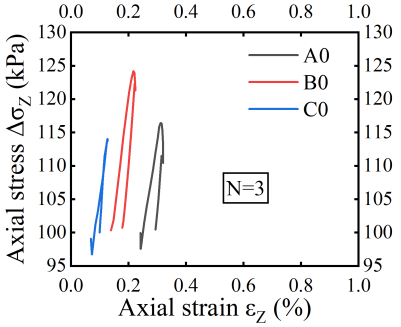
(b) Bi-directional PSR for typical cycle (N=10).



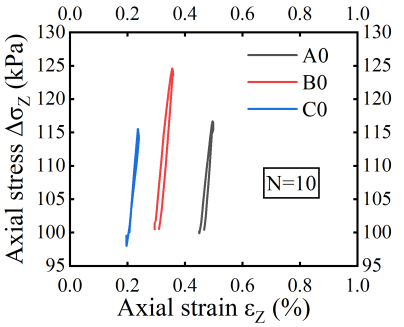
(c) Bi-directional PSR for typical cycle (N=1000).



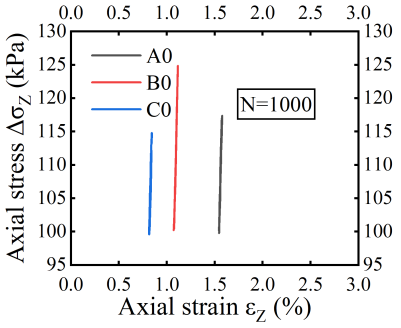
(d) Bi-directional PSR for typical cycle (N=5000).



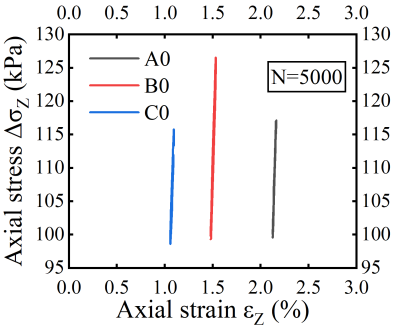
(e) Uni-directional PSR for typical cycle (N=3).



(f) Uni-directional for typical cycle (N=10).



(g) Uni-directional PSR for typical cycle (N=1000).



(h) Uni-directional PSR for typical cycle (N=5000).

Fig. 8 Axial stress-strain curves for typical loading cycles.

In conclusion, despite the direction of the shear stress (τ_{ZX} or τ_{ZY}), when the soil is subjected to periodic shear stress, it displays no strain accumulation. However, when the soil is under uni-directional shear stress, it will exhibit strain accumulation.

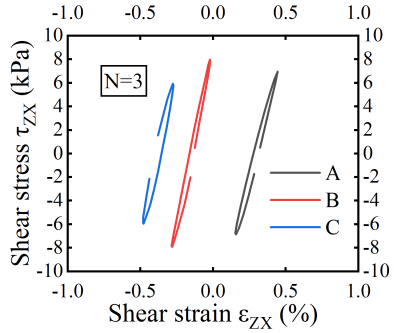
4.2 Dynamic axial strain analysis

In the VDDCSS, the axial displacement serves as a direct measure of specimen volume change due to the rigid lateral confinement. The high-resolution displacement sensor (resolution: 0.1 μm) ensures accurate monitoring of microscale deformations. Fig. 10 quantifies the progressive strain accumulation trajectory through 5,000 load cycles, revealing systematic permanent deformation mechanisms under cyclic traffic loading.

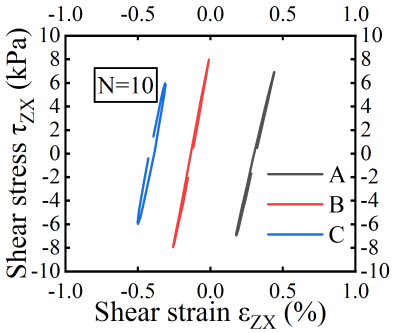
The vertical strain evolution of Paths A, A0, B, B0, C, and C0 is shown in Fig. 10(a), while Paths A-1, A0-1, B-1, B0-1, C-1, and C0-1 are detailed in Fig. 10(b). It can be seen from Fig. 10(a) that, Paths C and C0 exhibit a significantly lower ultimate vertical strain (maximum $\sim$1%) compared to Paths A and B, indicating that cyclic traffic loading markedly influences regions corresponding to points A (embankment center area) and B (embankment area under loaded line). In particular, Path A (bi-directional PSR) in Fig. 10(a) reaches 2.72%, versus 2.15% for Path A0 (uni-directional PSR), revealing 26.6% increase in the final strain. Similarly, Path B (bi-directional PSR) in Fig. 10(a) attains a final vertical strain of 2.41%, compared to 1.52% for Path B0 (uni-directional PSR), leading to 58.85% higher final strain. These quantitative contrasts demonstrate that bi-directional PSR induces remarkably larger vertical deformation than uni-directional PSR especially for Path B. Since Figs. 10(a) and 10(b) indicate similar ultimate vertical strains under both bi-directional and uni-directional PSR conditions at locations C, A-1, B-1, and C-1, but not A and B, it can be concluded that bi-directional PSR primarily influences the zones represented by points A and B. The reason can be concluded that, at shallow depths (vertical stress 100 kPa), initial shear stress significantly reduces settlement. However, at greater depths (vertical stress 200 kPa), the inhibiting effect becomes negligible as the high confining pressure dominates the response, with the minor deformation differences falling within experimental error. Furthermore, as shown in Fig. 10(a), the axial strain curves for Path A at 1 Hz and 0.8 Hz are nearly identical, indicating that the loading frequency (within the tested range) does not significantly affect the final accumulated strain under the given stress path.

When comparing Paths A and B, Paths A and B have similar shear stress paths and amplitudes and vertical stress paths, and Path B has a larger vertical stress amplitude. However, the final strain of Path B is smaller to that of Path A (2.41% versus 2.72%, both bi-directional PSR) because the initial shear stress of Path B limits the development of its vertical deformation. A similar conclusion can be drawn in the comparison of Paths A0 and B0 (2.15% versus 1.52%, both uni-directional PSR). It may be concluded that, the presence of initial shear stress partially inhibits the progression of vertical deformation under cyclic traffic loading.

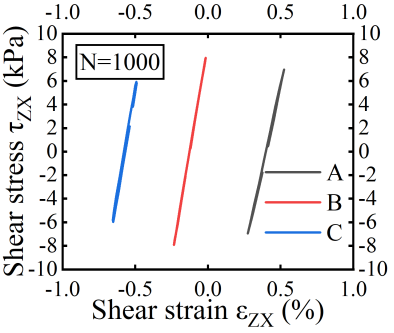
The evolution of the axial resilient modulus (M_Z), a key parameter for foundation performance [9, 56–59], is illustrated in Fig. 11. For all paths, M_Z exhibits an initial rapid reduction within the first 1000 cycles before stabilizing. Although the modulus ranges differ transiently among paths (e.g., Path A: 40–80 MPa; Path A0: 46–55 MPa),



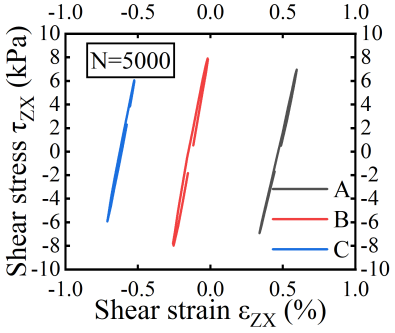
(a) Bi-directional PSR in X- direction for typical cycle (N=3).



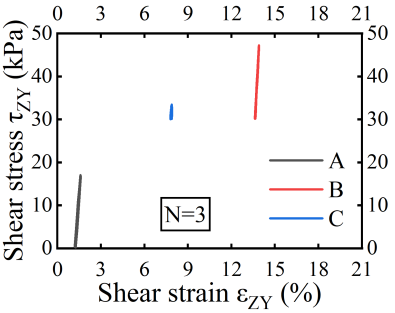
(b) Bi-directional PSR in X- direction for typical cycle (N=10).



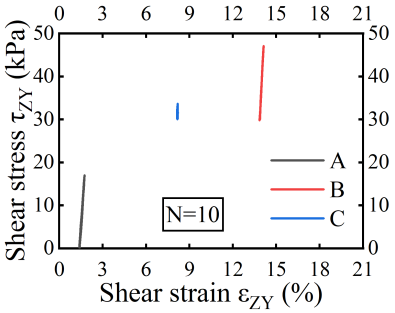
(c) Bi-directional PSR in X- direction for typical cycle (N=1000).



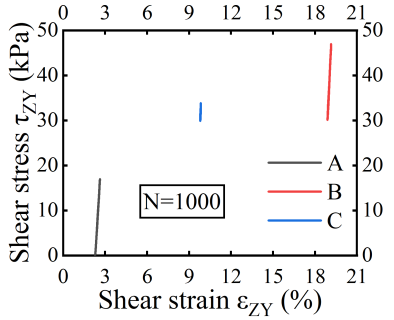
(d) Bi-directional PSR in X- direction for typical cycle (N=5000).



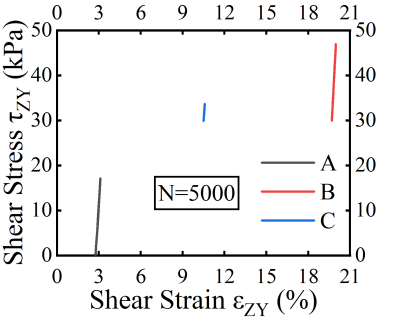
(e) Bi-directional PSR in Y- direction for typical cycle (N=3).



(f) Bi-directional in Y- direction for typical cycle (N=10).

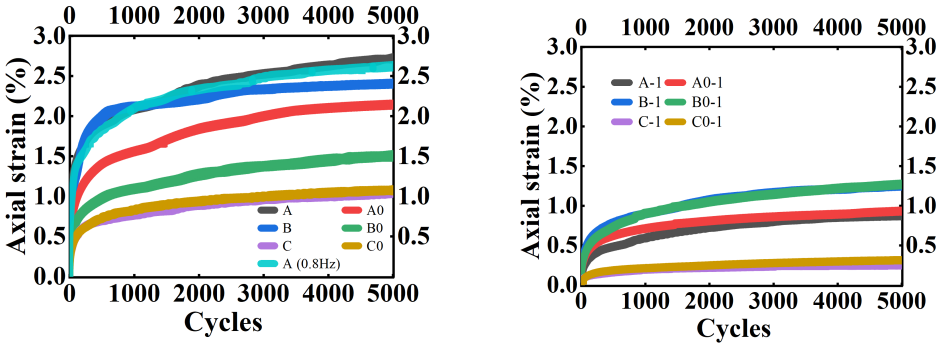


(g) Bi-directional PSR in Y- direction for typical cycle (N=1000).



(h) Bi-directional PSR in Y- direction for typical cycle (N=5000).

Fig. 9 Shear stress-strain curves for typical loading cycles.



(a) Path A, A0, B, B0, C and C0.

(b) Path A-1, A0-1, B-1, B0-1, C-1 and C0-1.

Fig. 10 Axial strain development for different stress paths.

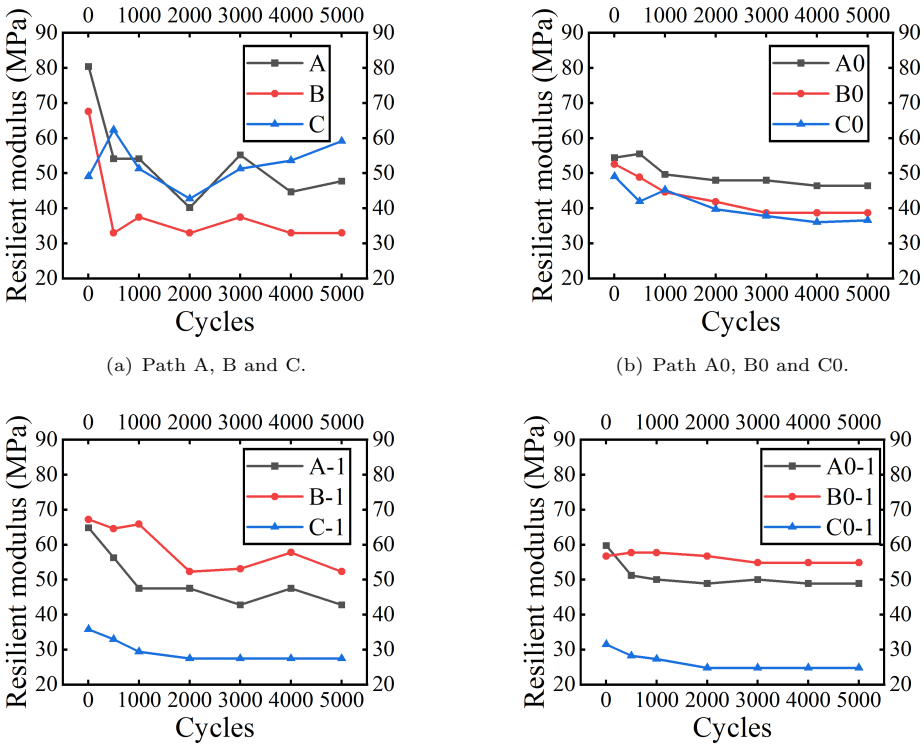
the long-term stabilized values under bi-directional PSR converge to levels equivalent to those under uni-directional PSR. This convergence indicates that PSR directionality has a negligible long-term influence on M_Z, aligning with prior observations [36, 60].

The axial plastic strain evolution throughout all loading cycles is shown in Fig. 12. A consistent pattern is observed: a sharp reduction occurs within the first 50 cycles, followed by gradual stabilization. Critically, bi-directional PSR generates higher cumulative plastic axial strain per cycle than uni-directional PSR during the initial loading phase (first 10 cycles), confirming its role in accelerating early deformation. After the initial ten cycles, the plastic strain rate remains below 0.02% per cycle for all paths, indicating rapid stabilization. This demonstrates that permanent axial deformation is predominantly governed by plastic strain accumulation.

The above analysis demonstrates that cyclic traffic loading induces permanent axial deformation primarily through plastic strain accumulation, with resilient deformation having negligible influence. Plastic deformation thus governs long-term axial displacement under repeated loading.

4.3 Analysis of shear strain behavior

Fig. 13 presents shear strain-cycle relationships for paths A, A0, B, and C. It can be seen from Figs. 13(a) and 13(b) that near-identical development patterns of shear strain along the X-direction (train driving orientation) under both bi-directional (Path A) and uni-directional PSR (Path A0) is observed. This convergence provides direct evidence of independent shear control mechanisms in the X- and Y-directions within VDDCSS. Due to the small stress amplitude, as well as the same stress waveform of Paths A-1, B-1 and C-1, only paths A, B and C were analyzed and shown in the figures. X-direction plastic shear strain accumulation remains highly suppressed in Paths A, A0, and B due to the cyclic cancellation of mechanical work between positive and negative τ_{ZX} phases within each loading cycle (standard sinusoidal waves). This self-stabilizing effect matches the reversing stress patterns in Figs. 5(a) and 5(b), and continues under different τ_{ZX} conditions (Figs. 13(b) and 13(c)). Consequently, when subjected to sinusoidal shear waveforms, instantaneous shear strain is governed



(a) Path A, B and C.

(b) Path A0, B0 and C0.

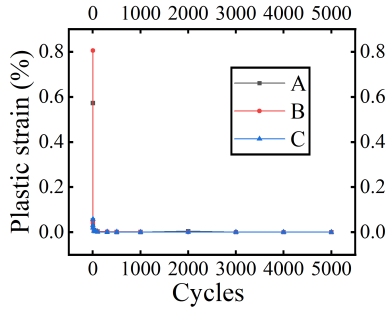
(c) Path A-1, B-1 and C-1.

(d) Path A0-1, B0-1 and C0-1.

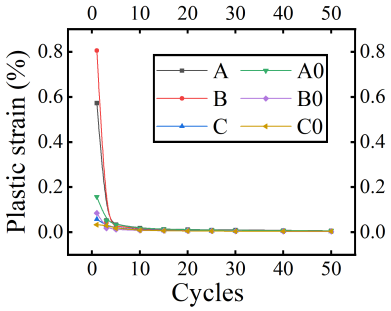
Fig. 11 The evolution of resilient modulus with increasing load cycles.

by stress magnitude, while continuous work cancellation suppresses long-term strain accumulation.

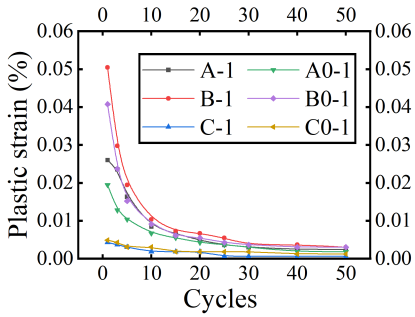
In contrast, as shown in Fig. 13(d), Path C exhibits minor (ranging between 0-1%) progressive accumulation of X-direction shear strain,. The strain accumulation is because in each loading cycle, the shear stress in the X-direction (τ_{ZX}) is almost uni-directional (positive), as shown in the waveform in Fig. 5(c), unlike the shear stress of Path A and B in the X-direction. For Paths A, B, and C with bi-directional PSR shown in Figs. 5(d), 5(e) and 5(f), similar conclusion can be drawn, in which the shear strain also accumulates in the Y direction. Thus, for uni-directional shear stress (persistently positive or negative), both the magnitude and progression of shear strain are stress-controlled. Bi-directional PSR loading progressively accumulates Y-direction permanent shear strain, mirroring established axial plastic strain behavior as experimentally confirmed.



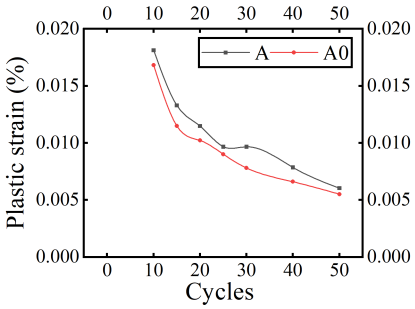
(a) Axial plastic strain development (N=5000).



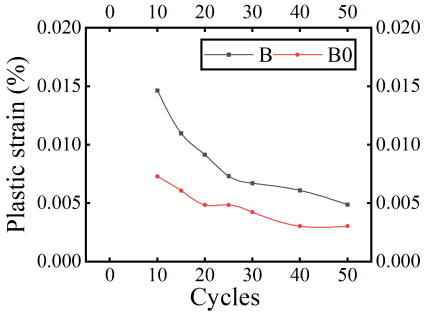
(b) Bi- and uni- PSR comparison (A-C) (N=50).



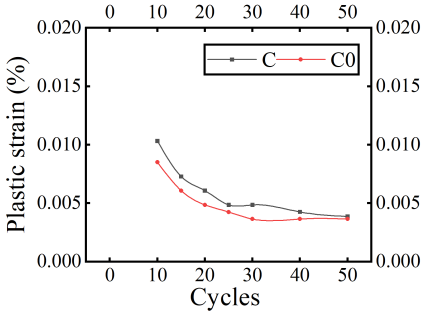
(c) Bi- and uni- PSR comparison (A-1-C-1) (N=50).



(d) Path A and A0 (N=50)



(e) Path B and B0 (N=50).

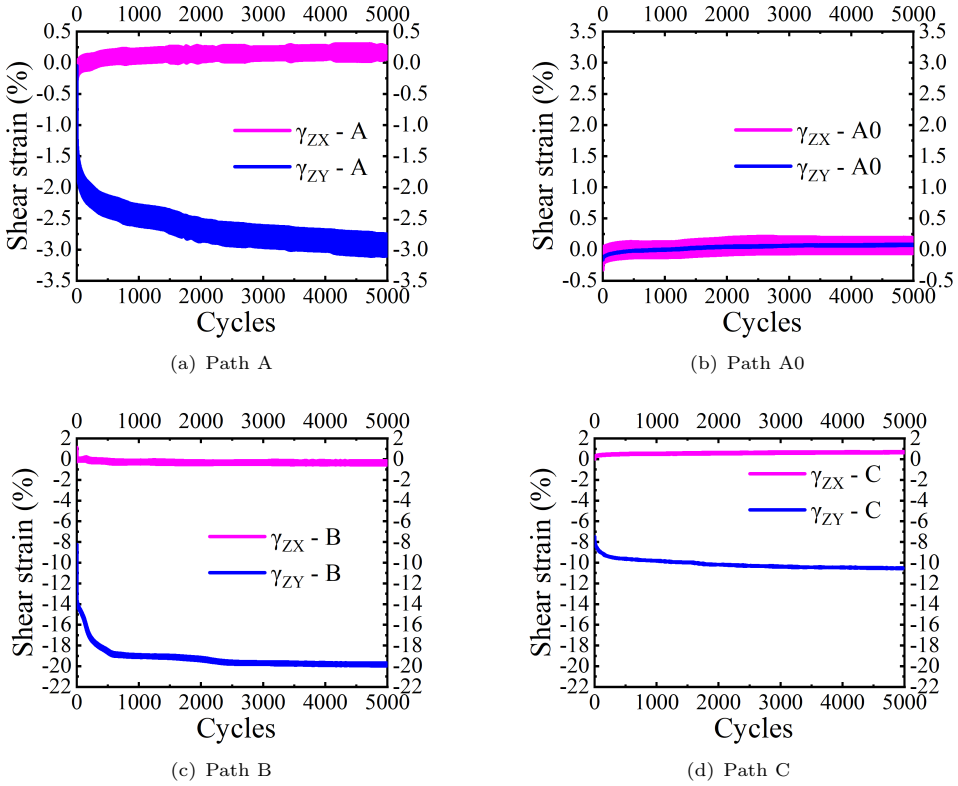


(f) Path C and C0 (N=50).

Fig. 12 Axial plastic strain evolution under varied loading paths at specified cycles (N).

5 Conclusion

This research employs FEM to extract critical stress paths from double track heavy haul railway embankment cross-sections under cyclic traffic loading. These simulated stress paths then drive VDDCSS experiments, explicitly comparing uni- and bi-directional PSR scenarios. The study systematically evaluates axial strain, shear



(a) Path A (b) Path A0

(c) Path B (d) Path C

Fig. 13 Shear strain development under different stress paths.

strain, resilient modulus, and plastic strain responses. Main findings are summarized below:

(1) During heavy-haul train crossings, embankments develop complex stress paths characterized by bi-directional PSR - spanning centerline, unloaded-track, and loaded-track zones - with PSR angle amplitude scaling proportionally to resultant shear stress magnitude.

(2) Bi-directional shear stresses induce dynamic PSR across multiple spatial planes, while uni-directional shear confines PSR to a single plane. This mechanistic divergence produces substantially greater vertical soil deformations under bi-directional PSR than uni-directional conditions. Therefore, bi-directional PSR modeling is essential for accurate vertical deformation prediction in cyclic traffic-loaded heavy-haul railway embankments.

(3) During long-term double track heavy haul train operations, soil under the railway embankment shows different degrees of vertical settlement at different locations. Among the three monitoring points, the largest settlement happens in the embankment centerline areas.

(4) The axial resilient modulus remains independent of PSR directionality, since resilient strains negligibly influence total axial deformation which is dominated by

plastic components. Significant greater accumulation of axial plastic strain develops under bi-directional PSR loading compared to uni-directional conditions.

(5) Periodic shear stress modulates instantaneous shear strain magnitude without permanent strain accumulation. In contrast, uni-directional shear loading governs both strain magnitude and its cumulative evolution.

(6) The initial shear stress induced by the embankment's self-weight mitigates the long-term vertical deformation resulting from cyclic traffic loading. The effect of the embankment's self weight on the long-term deformation should be taken into account in designing double track heavy haul embankments subjected to traffic loads.

This study has three main limitations. First, the laboratory experiments were conducted exclusively on a specific sand (Leighton Buzzard Sand, Fraction E). Consequently, the quantitative deformation results may differ for embankments composed of other soil types, especially cohesive soils, although the qualitative mechanism that bi-directional PSR induces greater deformation remains valid. Second, a methodological simplification was employed: due to apparatus constraints, the lateral stress was estimated using an empirical formula with a constant K0 assumption rather than being directly measured, which may affect the precision of the simulated stress paths. Third, the conclusions are derived from laboratory and numerical analysis and have not yet been validated against field long-term monitoring data. Future work should validate this mechanism in a wider range of typical embankment materials, develop experimental techniques capable of direct lateral stress measurement, and integrate the mechanism into constitutive models for practical performance prediction.

Funding. This work is supported by National Natural Science Foundation of China (Project code 11872219) and Ningbo Science and Technology Bureau (Project code 2023J189). Their financial support is greatly appreciated.

Conflict of Interest Statement. The authors declare that they have no known competing financial interests or personal relationships that could have appeared to influence the work reported in this paper.

Data Availability. The data that support the findings of this study are available from the corresponding author upon reasonable request.

Author Contribution. Weipin Wu: Methodology, Formal analysis, Writing - Original Draft, Conceptualization; Yung-Tsang Chen: Writing - Review & Editing, Supervision, Project administration, Funding acquisition, Visualization; Dariusz Wanatowski: Review & Editing, Supervision, Investigation.

References

[1] Ding, Y., Jia, Y., Zong, Z., Wang, X., Zhang, J., Chen, X.: Study on characteristics and mechanism of subgrade mud pumping under heavy-haul train loads. Bull Eng Geol Environ **83**(2), 63 (2024) https://doi.org/10.1007/s10064-024-03555-7

[2] Geng, Z., Li, X., Zhang, B.: Simulation study of heavy haul train operation on datong-qinhuangdao railway. China Railway Science **29**(2), 88–93 (2008)

[3] Lazorenko, G., Kasprzhitskii, A., Kukharskii, A., Kochur, A., Yavna, V.: Failure analysis of widened railway embankment with different reinforcing measures under heavy axle loads: A comparative fem study. Transportation Engineering **2**, 100028 (2020)

[4] Sabri, M.S., Ahmad, F., Samui, P., Verma, A.K., Kurup, P.U.: Effect of pore water pressure on slope stability in a heavy-haul railway embankment using a deep learning approach. Journal of Earth System Science **134**(2), 90 (2025)

[5] Wang, T., Yan, Z., Li, T., Wang, L., Luo, Q.: Design methodology for heavy-haul railway track foundations under 40-tonne axle loads. Int J Rail Transp, 1–16 (2025) https://doi.org/10.1080/23248378.2025.2453928

[6] Lovett, A.H.: Railroad decision support tools for track maintenance. PhD thesis, University of Illinois at Urbana-Champaign (2017)

[7] Martland, C.D.: Introduction of heavy axle loads by the north american rail industry. In: Journal of the Transportation Research Forum, vol. 52, pp. 103–125 (2013). https://doi.org/10.22004/ag.econ.207349

[8] Grabe, P., Clayton, C.: Permanent deformation of railway foundations under heavy axle loading. In: International Heavy Haul Association Conference (2003). http://eprints.soton.ac.uk/id/eprint/53878

[9] Lazorenko, G., Kasprzhitskii, A., Khakiev, Z., Yavna, V.: Dynamic behavior and stability of soil foundation in heavy haul railway tracks: A review. Constr Build Mater **205**, 111–136 (2019) https://doi.org/10.1016/j.conbuildmat.2019.01.184

[10] Gräbe, P., Clayton, C.: Effects of principal stress rotation on resilient behavior in rail track foundations. J Geotech Geoenviron Eng **140**(2), 04013010 (2014) https://doi.org/10.1061/(ASCE)GT.1943-5606.0001023

[11] Qian, J., Li, S., Gu, X., Zhang, J.: A unified model for estimating the permanent deformation of sand under a large number of cyclic loads. Ocean Eng **181**, 293–302 (2019) https://doi.org/10.1016/j.oceaneng.2019.03.051

[12] Ramos, A., Correia, A.G., Indraratna, B., Ngo, T., Calçada, R., Costa, P.A.: Mechanistic-empirical permanent deformation models: Laboratory testing, modelling and ranking. Transp Geotech **23**, 100326 (2020) https://doi.org/10.1016/j.trgeo.2020.100326

[13] Wang, M., Kong, L., Zhao, C., Zang, M.: Dynamic characteristics of lime-treated expansive soil under cyclic loading. J Rock Mech Geotech Eng **4**(4), 352–359 (2012) https://doi.org/10.3724/SP.J.1235.2012.00352

[14] Yoka, B., Morvan, M., Breul, P.: Characterization of the mechanical behavior of the fine soil of railway subgrade under heavy train loading. Bull Eng Geol Environ

82(10), 390 (2023) https://doi.org/10.1007/s10064-023-03401-2

[15] Fu, Z., Wang, G., Song, W., Yu, Y., Wei, P., Wu, T.: Deformation behavior of saturated soft clay under cyclic loading with principal stress rotation. Appl Sci **11**(19), 8987 (2021) https://doi.org/10.3390/app11198987

[16] Punetha, P., Nimbalkar, S.: Geotechnical rheological modeling of ballasted railway tracks considering the effect of principal stress rotation. Can Geotech J **59**(10), 1793–1818 (2022) https://doi.org/10.1139/cgj-2021-0562

[17] Wu, T., Jin, H., Guo, L., Sun, H., Tong, J., Jiang, Y., Wei, P.: Predicting method on settlement of soft subgrade soil caused by traffic loading involving principal stress rotation and loading frequency. Soil Dyn Earthquake Eng **152**, 107023 (2022) https://doi.org/10.1016/j.soildyn.2021.107023

[18] Bao, Z., Cui, X., Du, Y., Jin, Q., Hao, J., Cao, T., Li, X., Zhang, X.: Development and verification of subgrade service performance test system considering the principal stress rotation. Transp Geotech **50**, 101474 (2025) https://doi.org/10.1016/j.trgeo.2024.101474

[19] Mamou, A., Clayton, C., Powrie, W., Priest, J.: The role of clay content on the response of railway track foundations during free-to-drain cyclic changes in principal stress rotation. Transp Geotech **20**, 100246 (2019) https://doi.org/10.1016/j.trgeo.2019.100246

[20] Al-Rkaby, A.H., Chegenizadeh, A., Nikraz, H.: Cyclic behavior of reinforced sand under principal stress rotation. J Rock Mech Geotech Eng **9**(4), 585–598 (2017) https://doi.org/10.1016/j.jrmge.2017.03.010

[21] Gräbe, P.J.: Resilient and permanent deformation of railway foundations under principal stress rotation. PhD thesis, University of Southampton (2002)

[22] Li, T., Shu, J., Wu, B., Huang, J., Deng, Z.: Effect of different water contents on the softening characteristics of clay under intermittent cyclic dynamic loading. Bull Eng Geol Environ **83**(4), 108 (2024) https://doi.org/10.1007/s10064-024-03605-0

[23] Mamou, A.: Effects of principal stress rotation and drainage on the resilient stiffness of railway foundations. PhD thesis, University of Southampton (2013)

[24] Xiao, J., Juang, C.H., Wei, K., Xu, S.: Effects of principal stress rotation on the cumulative deformation of normally consolidated soft clay under subway traffic loading. J Geotech Geoenviron Eng **140**(4), 04013046 (2014) https://doi.org/10.1061/(ASCE)GT.1943-5606.0001069

[25] Yin, S., Liu, P., Kong, L., Zhang, X., Qi, Y., Huang, J.: Accumulated plastic strain behavior of granite residual soil under traffic loading. Soil Dyn Earthquake

Eng **164**, 107617 (2023) https://doi.org/10.1016/j.soildyn.2022.107617

[26] Zhang, M., Yang, Y., Zhang, H., Li, Q.: Granular behaviour under bi-directional shear with constant vertical stress and constant volume. J Rock Mech Geotech Eng **16**(10), 4300–4318 (2024) https://doi.org/10.1016/j.jrmge.2024.01.010

[27] Kammerer, A., Wu, J., Riemer, M., Pestana, J., Seed, R.: Shear strain development in liquefiable soil under bi-directional loading conditions. In: Proceedings, 13th World Conference on Earthquake Engineering, Paper, vol. 2081 (2004)

[28] Li, Y., Yang, Y., Yu, H.-S., Roberts, G.: Correlations between the stress paths of a monotonic test and a cyclic test under the same initial conditions. Soil Dyn Earthquake Eng **101**, 153–156 (2017) https://doi.org/10.1016/j.soildyn.2017.07.023

[29] Liu, F., Luo, P., Hu, X., Zhang, Y.: Effect of angle between initial and cyclic shear stress on behaviors of marine clay. Mar Georesour Geotechnol **36**(5), 617–624 (2018) https://doi.org/10.1080/1064119X.2017.1361489

[30] Shabani, F., Kaviani-Hamedani, F.: Cyclic response of sandy subsoil layer under traffic-induced principal stress rotations: Application of bidirectional simple shear apparatus. Soil Dyn Earthquake Eng **164**, 107573 (2023) https://doi.org/10.1016/j.soildyn.2022.107573

[31] Wang, J., Yang, Y., Yu, H.-S., Liu, E., Li, X., Wu, W.: Experimental study of the effects of initial shear stress on post-liquefaction behavior of submarine liquefiable ground: An energy-based evaluation. Appl Ocean Res **141**, 103755 (2023) https://doi.org/10.1016/j.apor.2023.103755

[32] Gräbe, P.J., Clayton, C.R.I., Shaw, F.J.: Deformation measurement on a heavy haul track formation. In: Proceedings of 8th International Heavy Haul Conference, pp. 287–295 (2005)

[33] Leng, W., Xiao, Y., Nie, R., Zhou, W., Liu, W.: Investigating strength and deformation characteristics of heavy-haul railway embankment materials using large-scale undrained cyclic triaxial tests. Int J Geomech **17**(9), 04017074 (2017) https://doi.org/10.1061/(ASCE)GM.1943-5622.0000956

[34] Zhao, Y., Yang, Y., Ling, X., Gong, W., Li, G., Su, L.: Dynamic behavior of natural sand soils and fiber reinforced soils in heavy-haul railway embankment under multistage cyclic loading. Transp Geotech **28**, 100507 (2021) https://doi.org/10.1016/j.trgeo.2020.100507

[35] Systèmes, D.: Simulia, abaqus/cae user's manual. ABAQUS Documentation V6.7 (2014)

[36] Li, X., Yang, Y., Wang, J., Yu, Q., Yu, H.: Deformation of pavement subgrade subjected to traffic loads considering multi-direction principal stress rotation. Soil Dyn Earthquake Eng **162**, 107480 (2022) https://doi.org/10.1016/j.soildyn.2022.107480

[37] Qian, J., Du, Z., Lu, X., Gu, X., Huang, M.: Effects of principal stress rotation on stress–strain behaviors of saturated clay under traffic–load–induced stress path. Soils Found **59**(1), 41–55 (2019) https://doi.org/10.1016/j.sandf.2018.08.014

[38] Shi, J., Burrow, M.P., Chan, A.H., Wang, Y.J.: Measurements and simulation of the dynamic responses of a bridge–embankment transition zone below a heavy haul railway line. Proc Inst Mech Eng, Part F: J Rail Rapid Transit **227**(3), 254–268 (2013) https://doi.org/10.1177/0954409712460979

[39] Yang, Q., Tang, Y., Yuan, B., Zhou, J.: Cyclic stress–strain behaviour of soft clay under traffic loading through hollow cylinder apparatus: effect of loading frequency. Road Mater Pavement Des **20**(5), 1026–1058 (2019) https://doi.org/10.1080/14680629.2018.1428219

[40] National Railway Administration of China, TB 10625-2017: Chinese Code for Design of Heavy Haul Railway. National Railway Administration of China

[41] Dong, J., Wu, Z.-H., Li, X., Chen, H.-Y.: Dynamic response and pile-soil interaction of a heavy-haul railway embankment slope reinforced by micro-piles. Computers and Geotechnics **100**, 144–157 (2018)

[42] Dong, L., Zhang, Q.-L., Cai, D., Ye, y.: Numerical analysis of dynamic deformation characteristics of ballasted track subgrade for high-speed and heavy-haul railways. China Railway Science (2), 6–11 (2010). In Chinese

[43] Krabbenhoft, S., Christensen, R.: Design of railway embankment using the mohr coulomb criterion and gsk model for cohesionless soil. In: Advances in Engineering Materials, Structures and Systems: Innovations, Mechanics and Applications, pp. 2292–2296. CRC Press, ??? (2019)

[44] Tang, Y., Xiao, S., Yang, Q.: Numerical study of dynamic stress developed in the high speed rail foundation under train loads. Soil Dyn Earthquake Eng **123**, 36–47 (2019) https://doi.org/10.1016/j.soildyn.2019.04.018

[45] Tan, F.: Centrifuge and theoretical modelling of conical footings on sand. Ph.D. thesis, Univ. of Cambridge (1990)

[46] Boulanger, R.W., Seed, R.B.: Liquefaction of sand under bidirectional monotonic and cyclic loading. J Geotech Eng **121**(12), 870–878 (1995) https://doi.org/10.1061/(ASCE)0733-9410(1995)121:12(870)

[47] Kim, Y.-S.: Static simple shear characteristics of nak-dong river clean sand. KSCE

J Civ Eng **13**, 389–401 (2009) https://doi.org/10.1007/s12205-009-0389-9

[48] Wood, D., Drescher, A., Budhu, M.: On the determination of stress state in the simple shear apparatus. Geotech Test J **2**(4), 211–222 (1979) https://doi.org/10.1520/GTJ10460J

[49] Jaky, J.: Pressure in silos. In: Proceeding of 2nd International Conference on Soil Mechanics, vol. 1, pp. 103–107 (1948)

[50] Kalman, E.: Determination of the coefficient of earth pressure at rest in situ in overconsolidated clay. In: World Tunnel Congress 2008-Underground Facilities for Better Environment and Safety–India, pp. 391–396 (2008)

[51] Lanzano, G., Visone, C., Bilotta, E., Magistris, F.: Experimental assessment of the stress–strain behaviour of leighton buzzard sand for the calibration of a constitutive model. Geotech Geol Eng **34**, 991–1012 (2016) https://doi.org/10.1007/s10706-016-0019-5

[52] Liu, J., Zhu, K., Shen, Y., Ren, Y., Zuo, J., Zhang, X.: Experimental investigation on the deformation and noncoaxial characteristics of fiber-reinforced aeolian soil under traffic load. Int J Geomech **22**(5), 04022054 (2022) https://doi.org/10.1061/(ASCE)GM.1943-5622.0002364

[53] Lu, Z., Fang, R., Yao, H., Hu, Z., Liu, J.: Evaluation and analysis of the traffic load–induced settlement of roads on soft subsoils with low embankments. Int J Geomech **18**(6), 04018043 (2018) https://doi.org/10.1061/(ASCE)GM.1943-5622.0001123

[54] Qian, J., Wang, Y., Huang, M., Xue, J.: Experimental identification of plastic shakedown behaviors of saturated clay subjected to traffic loading. In: Zhang, X. (ed.) Soil Behavior and Geomechanics, pp. 353–362. American Society of Civil Engineers, ??? (2014)

[55] Tang, L., Chen, H., Sang, H., Zhang, S., Zhang, J.: Determination of traffic-load-influenced depths in clayey subsoil based on the shakedown concept. Soil Dyn Earthquake Eng **77**, 182–191 (2015) https://doi.org/10.1016/j.soildyn.2015.05.009

[56] Blackmore, L., Clayton, C.R., Powrie, W., Priest, J.A., Otter, L.: Saturation and its effect on the resilient modulus of a pavement formation material. Géotechnique **70**(4), 292–302 (2020) https://doi.org/10.1680/jgeot.18.P.053

[57] Khoury, N.N., Zaman, M.M.: Correlation between resilient modulus, moisture variation, and soil suction for subgrade soils. Transp Res Rec **1874**(1), 99–107 (2004) https://doi.org/10.3141/1874-11

[58] Nie, R., Sun, B., Leng, W., Li, Y., Ruan, B.: Resilient modulus of coarse-grained

subgrade soil for heavy-haul railway: An experimental study. Soil Dyn Earthquake Eng **150**, 106959 (2021) https://doi.org/10.1016/j.soildyn.2021.106959

[59] Thevakumar, K., Indraratna, B., Ferreira, F.B., Carter, J., Rujikiatkamjorn, C.: The influence of cyclic loading on the response of soft subgrade soil in relation to heavy haul railways. Transp Geotech **29**, 100571 (2021) https://doi.org/10.1016/j.trgeo.2021.100571

[60] Wang, J., Zhou, Z., Hu, X., Guo, L., Cai, Y.: Effects of principal stress rotation and cyclic confining pressure on behavior of soft clay with different frequencies. Soil Dyn Earthquake Eng **118**, 75–85 (2019) https://doi.org/10.1016/j.soildyn.2018.12.013